

Fully developed turbulent dynamo at low magnetic Prandtl numbers.

Rodion Stepanov †

Institute of Continuous Media Mechanics,
Korolyov 1, 614013 Perm, Russia

Franck Plunian ‡

Laboratoires des Ecoulements Géophysiques et Industriels,
B.P. 53, 38041 Grenoble Cedex 9, France

(September 19, 2018)

We investigate the dynamo problem in the limit of small magnetic Prandtl number (Pm) using a shell model of magnetohydrodynamic turbulence. The model is designed to satisfy conservation laws of total energy, cross helicity and magnetic helicity in the limit of inviscid fluid and null magnetic diffusivity. The forcing is chosen to have a constant injection rate of energy and no injection of kinetic helicity nor cross helicity. We find that the value of the critical magnetic Reynolds number (Rm) saturates in the limit of small Pm . Above the dynamo threshold we study the saturated regime versus Rm and Pm . In the case of equipartition, we find Kolmogorov spectra for both kinetic and magnetic energy except for wave numbers just below the resistive scale. Finally the ratio of both dissipation scales (viscous to resistive) evolves as $Pm^{-3/4}$ for $Pm < 1$.

1 Introduction

Most of astrophysical bodies possess or have had in their history their own magnetic fields. In most cases their generation rely on inductive processes produced by the turbulent motion of the electroconducting fluid within the body [1]. An important parameter of the problem is the magnetic Prandtl number defined by $Pm = \nu/\eta$ where ν is the viscosity and η the magnetic diffusivity of the fluid. In the “magnetic” universe Pm varies from values as large as 10^{14} for the interstellar medium [2] to values as small as 10^{-6} for the iron core of planets or stellar plasmas. This large spectrum of possible Pm values implies strong differences between possible generation mechanisms. In some sense Pm is a measure of the kinetic energy spectrum available for

† rodion@icmm.ru

‡ Franck.Plunian@hmg.inpg.fr; <http://legi.hmg.inpg.fr/~plunian>

generating magnetic energy. When $\text{Pm} \geq 1$ the resistive scale is smaller than the viscous scale implying that all velocity scales are available for generating some magnetic field. In the other hand for $\text{Pm} < 1$, only the velocity scales larger than the resistive scale are available for the magnetic field generation. In that case, the velocity scales smaller than the resistive scale are enslaved to the larger scales and in essence they stay passive in the generation process. Besides this is why the large eddy simulation technique may be recommended in that case [3]. Therefore, at first sight one can expect that dynamo action is all the more difficult to obtain since Pm is smaller in reason of a smaller velocity spectrum available for the magnetic generation. This is indeed what comes out from recent numerical simulations [4, 5, 6, 7, 8, 9] (see also [10] and references therein for an alternative approach). Though, we have evidence of magnetic field in planets and stars, and dynamo action has also been reproduced in experiments working with liquid sodium for which Pm is small ($\sim 10^{-6}$) [11, 12, 13, 14]. These experiments and further devices in preparation [15, 16, 17] are designed in such a way that the dynamo mechanism is produced by the large scale of the flow due to an appropriate large scale forcing. The turbulence naturally developing at smaller scales may play a role though this is still unclear [18, 19, 3, 20, 21]. In these experiments, the choice of the forcing is based on the hypothesis that it is the stationary part of the large scale flow which should be important for the generation mechanism. A number of flow geometries studied in the past turned out to be good candidates for such experiments [22, 23, 24].

In the present paper we are interested in the possibility for a Kolmogorov type turbulent flow to generate dynamo action at low Pm , without need for a large scale motion controlling the generation mechanism. We expect the eddies having the highest shearing rate to be the more active for generating the magnetic field, at least during the kinematic stage of magnetic field growth. As in Kolmogorov turbulence $u_l/l \approx l^{-2/3}$, these eddies correspond to the smallest available scale which is the viscous scale for $\text{Pm} \geq 1$ [25] and the resistive scale for $\text{Pm} < 1$ [9]. Eventually the magnetic field will then spread out to larger scales due to the nonlinear interactions. This problem is hard to solve by direct numerical simulation for it needs high resolution in order to describe magnetic phenomena adequately [26]. Some results have been obtained using the EDQNM closure applied to the MHD equations [27] near the critical Rm and for arbitrary low values of Pm . Here we want to investigate arbitrary large values of Rm and small values of Pm . For that we use a shell model of MHD turbulence introduced by Frick and Sokoloff [28]. This model is the successor of several other shell models for MHD turbulence [29, 30, 31, 32, 33, 34, 35] but it is the only one to conserve all integrals of motions including magnetic helicity (or kinetic helicity for the non magnetic case). It is based on the so-called GOY hydrodynamic shell model [36, 37, 38, 39]. In [28], Frick and Sokoloff have

derived a model which represents either 2D or 3D MHD turbulence, depending on the choice of two parameters. As in real MHD turbulence the 2D model leads to the impossibility of dynamo action [40]. This shows that in spite that such a shell model is a drastic simplification of the real MHD turbulence, ignoring for example the geometrical structures of the motion and magnetic field, it contains enough features to make the difference between the 2D and 3D problems (see also [41]). It also reproduces quite well the structure functions at different orders of real MHD turbulence. Here we consider only the 3D model herein after referred to as FS98. This model has also been used by Lozhkin *et al.* [42] to show that small scale dynamo is possible at low Pm , contrary to the hypothesis put forward by Batchelor [43].

Giulani and Carbone [41] have shown that long runs with the FS98 model lead inevitably towards a “dynamical alignment” stopping the nonlinear transfer towards the smaller scales. Giulani and Carbone [41] suggested that this problem might be overcome with an other choice of the external driving force. This is what we have done here, adopting a forcing in such a way that it acts on several scales and depends on time with a random phase at each forcing scale (see section 2.2). Finally, we took care to have long runs well beyond any transient state, in order to have good statistics and reliable results.

2 Shell model for MHD turbulence

2.1 Model equations

The shell model is built up by truncation of the Navier-Stokes and induction equations. We define logarithmic shells, each shell being characterized by one real wave number $k_n = k_0 \lambda^n$ and dynamical complex quantities U_n and B_n representative of the velocity and magnetic fluctuations for wave vectors of norm ranging between k_n and k_{n+1} . The parameter λ is taken equal to the gold number $(1 + \sqrt{5})/2$ for it optimizes the resolution [44]. The model is described by the following set of equations ($0 \leq n \leq N$)

$$\begin{aligned} d_t U_n &= ik_n(Q_n(U, U, a) - Q_n(B, B, a)) \\ &\quad - \nu k_n^2 U_n + F_n, \end{aligned} \tag{1}$$

$$\begin{aligned} d_t B_n &= ik_n(Q_n(U, B, b) - Q_n(B, U, b)) \\ &\quad - \eta k_n^2 B_n, \end{aligned} \tag{2}$$

where

$$Q_n(X, Y, c) = c_1 X_{n+1}^* Y_{n+2}^* + c_2 X_{n-1}^* Y_{n+1}^*$$

$$+ c_3 X_{n-2}^* Y_{n-1}^*. \quad (3)$$

represents the nonlinear transfer rates with the four neighbouring shells $n-2$, $n-1$, $n+1$ and $n+2$. In addition we have to take $U_{-2} = U_{-1} = U_{N+1} = U_{N+2} = 0$ and $B_{-2} = B_{-1} = B_{N+1} = B_{N+2} = 0$. The parameter F_n is the forcing at shell n . The time unit is defined by the turnover time of the largest scale $\tau = (|U_0|k_0)^{-1}$. To determine the complex coefficients a_j and b_j , $j = 1, 2, 3$ we apply the property that the total energy E_{tot} , cross-helicity \mathcal{H}_C and magnetic helicity \mathcal{H}_B must be conserved in the limit of non-viscous and non-resistive limit $\nu = \eta = 0$. In our shell model, these quadratic quantities write in the following form

$$E_{tot} = \frac{1}{2} \sum_{n=0}^N (|U_n|^2 + |B_n|^2), \quad (4)$$

$$\mathcal{H}_C = \frac{1}{2} \sum_{n=0}^N (U_n B_n^* + B_n U_n^*), \quad (5)$$

$$\mathcal{H}_B = \frac{1}{2} \sum_{n=0}^N (-1)^n |B_n|^2 / k_n, \quad (6)$$

leading to $a_1 = 1$, $a_2 = (1 - \lambda)\lambda^{-2}$, $a_3 = -\lambda^{-3}$, $b_1 = b_2 = b_3 = (\lambda(1 + \lambda))^{-1}$. In the pure hydrodynamic case ($B_n = 0$) the original GOY model is recovered satisfying, in addition to (4), the conservation of the kinetic helicity [45]

$$\mathcal{H}_U = \frac{1}{2} \sum_{n=0}^N (-1)^n |U_n|^2 k_n. \quad (7)$$

2.2 Forcing and initial conditions

The forcing is chosen in order to control the injection rate of kinetic energy, cross and kinetic helicities. For that we spread the forcing on three neighbouring shells $n_f, n_f + 1$ and $n_f + 2$ with $F_{n_f+j} = f_j e^{i\phi_j}$, $j = 0, 1, 2$ where the f_j are positive real quantities and where the $\phi_j \in [0, 2\pi]$ are random phases. In that case the forcing is δ -correlated. Alternatively we also used a forcing for which the phases ϕ_j are constant during a certain time τ_c , which can be interpreted as a finite correlation time. In fact this does not make much difference either on the autocorrelation functions of U_n nor on the subsequent results. Therefore it is sufficient to use random phases. As we are interested to inject

neither kinetic helicity nor cross-helicity, the forcing functions must satisfy

$$\frac{1}{2} \sum_{n=n_f}^{n_f+2} U_n^* F_n + U_n F_n^* = \varepsilon, \quad (8)$$

$$\sum_{n=n_f}^{n_f+2} (-1)^n k_n (U_n^* F_n + U_n F_n^*) = 0, \quad (9)$$

$$\sum_{n=n_f}^{n_f+2} B_n^* F_n + B_n F_n^* = 0. \quad (10)$$

where ε is the rate of kinetic energy supplied to the system. Therefore for a given set of random ϕ_j ($j = 0, 1, 2$), the f_j depend on the U_j and B_j ($j = 0, 1, 2$) which expressions are given in Appendix. For some arbitrary initial conditions on U_j ($j = 0, 1$) of small intensity ($\sim 10^{-6}$) we let the hydrodynamic evolve until it reaches some statistically stationary state. Then introducing at a given time some arbitrary non zero values of B_j ($j = 0, 1$) of small intensity ($\sim 10^{-6}$) we solve the full problem until a statistically stationary MHD state is reached. The time of integration needed to obtain good statistics depends on ν and η but typically it is equal to several hundreds of the large scale turn-over time.

2.3 Input and output

The input parameters of the problem are ν , η , the forcing shell n_f , the rate of injected kinetic energy ε and the number of shells N . In the rest of the paper we take $\varepsilon = 1$.

As output we define the kinetic and magnetic energy for the shell n by

$$E^U(n) = \frac{1}{2} |U_n|^2 \quad \text{and} \quad E^B(n) = \frac{1}{2} |B_n|^2, \quad (11)$$

the total kinetic and total magnetic energy by

$$E_U = \sum_{n=0}^N E^U(n) \quad \text{and} \quad E_B = \sum_{n=0}^N E^B(n) \quad (12)$$

and the total energy by

$$E_{tot} = E_U + E_B. \quad (13)$$

Following [46] we define the spectral energy fluxes from the inside of the U (or B)-sphere (shells with $k < k_n$) to the outside of the U (or B)-sphere (shells with $k \geq k_n$). We note for example $\Pi_{U>}^{B<}(n)$ the energy flux from the inside of the B -sphere to the outside of the U -sphere. Then we have

$$\Pi_{U>}^{U<}(n) = \sum_{j=0}^{n-1} \Im\{k_j U_j^* Q_j(U, U, a)\} \quad (14)$$

$$\Pi_{U>}^{B<}(n) = \sum_{j=0}^{n-1} \Im\{-k_j U_j^* Q_j(B, B, a)\} \quad (15)$$

$$\Pi_{B>}^{U<}(n) = \sum_{j=0}^{n-1} \Im\{-k_j B_j^* Q_j(B, U, b)\} \quad (16)$$

$$\Pi_{B>}^{B<}(n) = \sum_{j=0}^{n-1} \Im\{k_j B_j^* Q_j(U, B, b)\}. \quad (17)$$

In FS98 the time average of $\Pi_{U>}^{U<}(n)$ is denoted Π_n . We also define the energy fluxes from the inside of the U - and B -spheres to the outside of the U -sphere or B -sphere by

$$\Pi_U(n) = \Pi_{U>}^{U<}(n) + \Pi_{U>}^{B<}(n) \quad (18)$$

$$\Pi_B(n) = \Pi_{B>}^{U<}(n) + \Pi_{B>}^{B<}(n) \quad (19)$$

and the total energy flux by

$$\Pi_{tot}(n) = \Pi_U(n) + \Pi_B(n). \quad (20)$$

We define the viscous and resistive dissipation rates $D^U(n)$ and $D^B(n)$ in shell n , by

$$D^U(n) = \nu k_n^2 |U_n|^2 \quad (21)$$

$$D^B(n) = \eta k_n^2 |B_n|^2 \quad (22)$$

and the total dissipation rate by

$$D_{tot} = \sum_{n=0}^N (D^U(n) + D^B(n)). \quad (23)$$

With these definitions we obtain the following shell-by-shell energy budget equations:

$$d_t \sum_{j=0}^n E^U(j) + \Pi_U(n) = - \sum_{j=0}^n D^U(j) + \epsilon \quad (24)$$

$$d_t \sum_{j=0}^n E^B(j) + \Pi_B(n) = - \sum_{j=0}^n D^B(j). \quad (25)$$

For a statistical stationary solution ($d_t \langle E^U(j) \rangle = d_t \langle E^B(j) \rangle = 0$) we have then

$$\langle \Pi_{tot}(n) \rangle = - \sum_{j=0}^n \langle D^U(j) \rangle - \sum_{j=0}^n \langle D^B(j) \rangle + \epsilon. \quad (26)$$

where here and after $\langle \ \rangle$ denotes time averaged quantities.

We define the kinetic and magnetic Reynolds numbers as

$$Re = \langle E_{tot} \rangle^2 / (\nu \langle D_{tot} \rangle) \quad (27)$$

$$Rm = \langle E_{tot} \rangle^2 / (\eta \langle D_{tot} \rangle). \quad (28)$$

Finally, following [47], we define the viscous (resp. resistive) scale k_ν^{-1} (resp. k_η^{-1}) as the one at which the viscous (resp. Ohmic) decay time $\tau_\nu = (\nu k_n^2)^{-1}$ (resp. $\tau_\eta = (\eta k_n^2)^{-1}$) becomes comparable to the typical turn-over time $\tau_U = (k_n \langle |U_n|^2 \rangle^{1/2})^{-1}$.

3 Hydrodynamics

Choosing the appropriate forcing corresponding to $B_n = 0$ we present in Fig.1 some results concerning the pure hydrodynamic case for $\nu = 10^{-8}$ and $n_f = 8$. In this case the forcing is δ -correlated. Though the autocorrelation function, defined by

$$cor(n, \tau) = \frac{\int U_n^*(t) U_n(t + \tau) + U_n(t) U_n^*(t + \tau) dt}{2 \sqrt{\int U_n^*(t) U_n(t) dt \int U_n(t + \tau) U_n^*(t + \tau) dt}} \quad (29)$$

and plotted in Fig.1a, is far from being the one of a δ -correlated velocity contrary to the Kasantzev model [9]. We also made comparisons with a finite

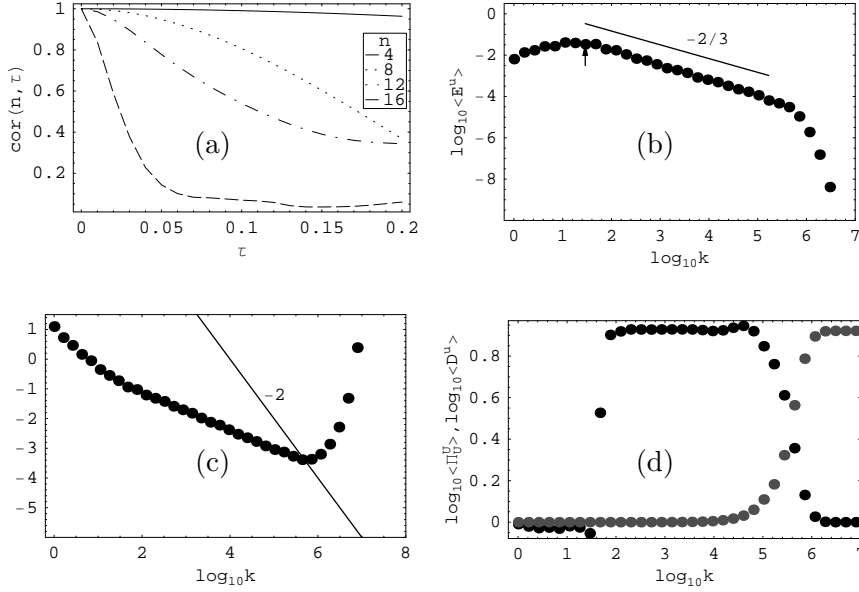


Figure 1. Hydrodynamic case for $\nu = 10^{-8}$ and a forcing scale (arrow) corresponding to $n_f = 8$. The output Reynolds number is $Re = 8 \cdot 10^7$. In (a), the autocorrelation function $cor(n, \tau)$ for a δ -correlated forcing is plotted versus τ and for several shells n . In (c), the turn-over (black dots) and dissipation (straight line) characteristic times are plotted versus $\log_{10} k$. In (b), the energy spectrum is plotted versus $\log_{10} k$ and the $k^{-2/3}$ slope (full line) is plotted for comparison. In (d), the energy flux (black dots) and the dissipation $\sum_{j=0}^n D^U(j)$ (gray dots) are plotted versus $\log_{10} k$.

correlation time forcing without finding any significant differences. Therefore the δ -correlated forcing does not seem to be an issue in our problem.

The kinetic energy spectrum (Fig.1b, black dots) of the stationary statistical state is found to be in $k^{-2/3}$ (which corresponds to a Fourier energy spectrum of $k^{-5/3}$ as expected in Kolmogorov turbulence). In Fig.1c, the spectral flux $\Pi_U(n)$ (black dots) and the dissipation $\sum_{j=0}^n D^U(j)$ (gray dots) are found to satisfy the kinetic energy budget (24) with $\epsilon = 1$. In addition, in the inertial range we find that $\Pi_U(n) \sim \epsilon$ and $\sum_{j=0}^n D^U(j) \sim 0$ as predicted by a Kolmogorov turbulence. After the viscous scale, $\Pi_U(n) \sim 0$ and $\sum_{j=0}^n D^U(j) \sim \epsilon$.

As previously defined, the viscous scale is the one at which the viscous decay time $\tau_\nu = (\nu k_n^2)^{-1}$ (full curve of Fig.1c) becomes comparable to the typical turn-over time $\tau_U = (k_n U_n)^{-1}$ (black dots of Fig.1c). This leads to $k_\nu \sim 10^6$ and compares indeed very well with the Kolmogorov dissipation scale $k_\nu^{-1} \sim (\nu^3/\epsilon)^{1/4}$. Finally the little bump of $\Pi_U(n)$ (black dots Fig.1d) just before the viscous scale looks like a bottle-neck effect [48].

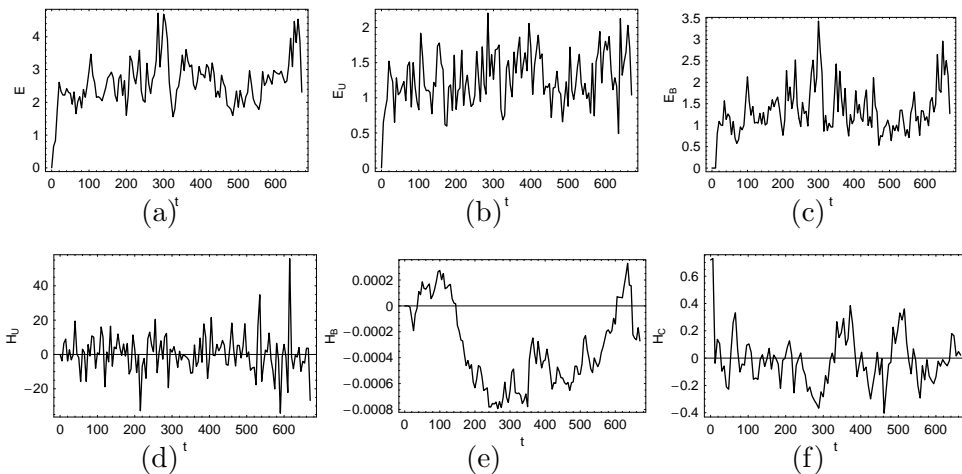


Figure 2. Quadratic quantities (a) E_{tot} , (b) E_U , (c) E_B , (d) \mathcal{H}_U , (e) \mathcal{H}_B and (f) $\mathcal{H}_C/\sqrt{E_U E_B}$ versus time, for $\nu = 10^{-9}$ and $\eta = 10^{-6}$.

4 Dynamo action

4.1 Time evolution of quadratic quantities

Here we start with a typical example of magnetic generation for $\nu = 10^{-9}$ and $\eta = 10^{-6}$ ($Pm = 10^{-3}$). In Fig. 2 the different quadratic quantities defined in (4), (5), (6), (7) and (12) are plotted versus time. A coarse time sampling has been chosen here for a better representation of the results and is not relevant of the actual time step used for the numerical calculations. The kinetic, magnetic and total energies have reached a statistical stationary steady state after a few hundred time steps. The fluctuations of these quantities are quite important due to the small values of ν and η . The kinetic helicity though its average is close to zero, shows strong fluctuations. In the other hand the magnetic helicity stays very small. Finally the relative cross helicity defined by $\mathcal{H}_C/\sqrt{E_U E_B}$ oscillates around zero. The fact that this latter quantity does not reach an asymptotic limit of ± 1 shows that there is no “dynamical alignment”. Therefore we are confident that our choice of forcing overcomes the problem raised by Giuliani and Carbone [41].

4.2 Spectrum analysis

In Fig. 3 we show the kinetic and magnetic spectrum at four successive times for again $\nu = 10^{-9}$ and $\eta = 10^{-6}$ ($Pm = 10^{-3}$). Each snapshot corresponds to an average over a not so large amount of time which explains why at early time the kinetic spectrum is not very smooth at large scales. In the early time, when the magnetic field is still not significant, the kinetic energy spectrum has

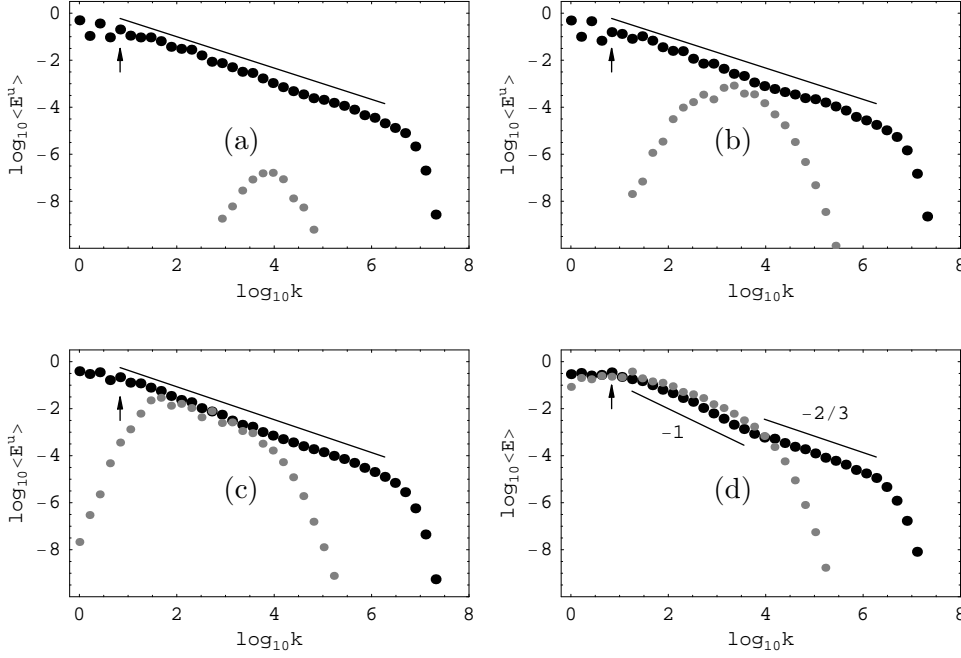


Figure 3. Kinetic (black dots) and magnetic (gray dots) spectra at four successive times (from (a) to (d)) for $n_f = 4$, $\nu = 10^{-9}$ and $\eta = 10^{-6}$. See also the movie energy1.mpg in which $\log_{10} E^U(n)$ and $\log_{10} E^B(n)$ are plotted versus $\log_{10} k$ with respectively red and blue dots.

a slope in $k^{-2/3}$ (corresponding to a Fourier spectrum in $k^{-5/3}$). Then, as Rm is much larger than the critical value of the dynamo instability, the magnetic energy starts to grow (Fig. 3a). We expect magnetic energy to be initially amplified by the eddies having the highest shearing rate, i.e. the smallest scale eddies. As $Pm < 1$, the smallest eddies available for dynamo action correspond to eddies at resistive scale. This is indeed what we find, as here, the resistive scale (defined as in section 2.3) corresponds to $\log_{10} k_\eta \sim 4.1$. We note that the Kolmogorov resistive scale given by $k_\eta \sim (\epsilon/\eta^3)^{1/4}$ (see section 4.3) with $\eta = 10^{-6}$, leads to a slightly higher value $\log_{10} k_\eta \sim 4.5$.

As Rm is sufficiently large, at subsequent times the magnetic energy reaches the level of kinetic energy (Fig. 3c). At that time the kinetic spectrum is not influenced yet by the nonlinear feedback of the magnetic field and is still in $k^{-2/3}$. Then the dynamical equilibrium between the magnetic and velocity fields settles down (Fig. 3d). A striking feature of this equilibrium is the change of slope (from $-2/3$ to ~ -1) of the kinetic energy spectrum for $k \leq k_\eta$ while the magnetic spectrum is slightly above the kinetic spectrum. We also note that the viscous dissipation scale has increased (the right part of the kinetic spectrum drifting to the left). This probably comes from the fact that there

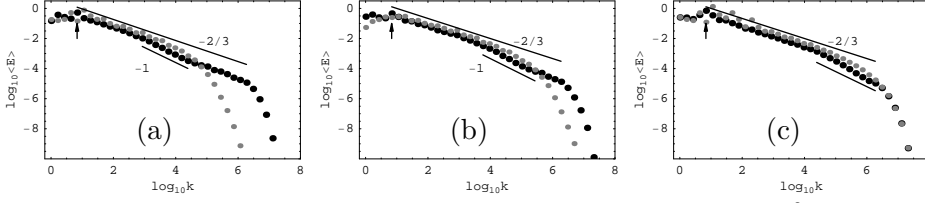


Figure 4. Kinetic (black dots) and magnetic (gray dots) spectra for $\nu = 10^{-9}$ and for Pm = (a) 10^{-2} , (b) 10^{-1} , (c) 10^0 and Re = (a) $6.5 \cdot 10^9$, (b) $4.4 \cdot 10^9$, (c) $4.4 \cdot 10^9$. The forcing scale corresponds to $n_f = 4$.

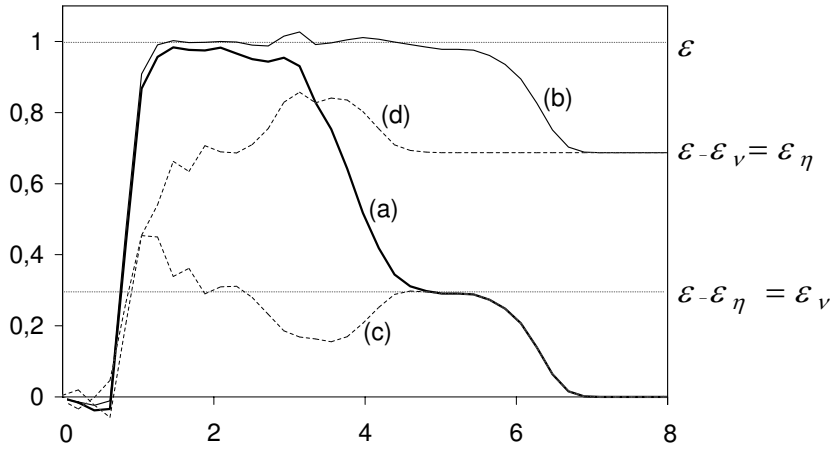


Figure 5. Spectral energy fluxes (a) $\Pi_{tot}(n)$, (b) $\Pi_U(n)$, (c) $\Pi_U^{U<}(n)$, (d) $\Pi_U^{B<}(n)$ versus $\log_{10} k$ for $\nu = 10^{-9}$ and Pm = 10^{-3} .

is less energy to dissipate by viscosity than at earlier time because of the additional Joule dissipation.

When changing the value of Pm while keeping the same value of ν and calculating again the final statistically stationary state, we observe again (Fig. 4) a deviation of the kinetic energy slope from $-2/3$ to ~ -1 whatever the value of Pm. To understand better these spectra, we plotted several fluxes in Fig. 5, for $\nu = 10^{-9}$ and Pm = 10^{-3} .

Looking at curve (a) which represents the total flux $\Pi_{tot}(n)$ versus $\log_{10} k$, one can distinguish three plateaus: the first one corresponds to scales larger than the resistive scale ($1 \leq \log_{10} k \leq 3$), the second one for scales smaller than the resistive scale but larger than the viscous scale ($\log_{10} k \sim 5$), and the third one for scales smaller than the viscous scale ($\log_{10} k \geq 7$). The drop from the first to the second plateau corresponds to the ohmic dissipation rate

$\epsilon_\eta = \sum_{j=0}^N D^B(j)$. The drop from the second to the third plateau corresponds to the viscous dissipation rate $\epsilon_\nu = \sum_{j=0}^N D^U(j)$. We clearly have $\epsilon = \epsilon_\nu + \epsilon_\eta$ as expected from (26) for $n = N$.

The curve (b) corresponds to $\Pi_U(n)$ versus $\log_{10} k$ with two plateaus, depending if the scale is larger or smaller than the viscous scale. The first plateau ($k \leq 6$) corresponds to $\Pi_U(n) \sim \epsilon$ and the second one ($k \geq 7$) to $\Pi_U(n) \sim \epsilon - \epsilon_\nu = \epsilon_\eta$. In particular, there is no clear change of $\Pi_U(n)$ just before the resistive scale that could explain the change of slope of the kinetic energy spectrum as previously pointed out.

Now let us have a look at curve (c). The transfer rate $\Pi_{U>}^{U<}(n)$ is responsible for the direct cascade of kinetic energy and would be constant leading to a Kolmogorov spectrum if the magnetic field was null (see Fig. 1). This would remain true for a non zero magnetic field only if the curve (c) was staying flat with $\Pi_{U>}^{U<}(n) = \epsilon_\nu$ for $2 < \log_{10} k < 5.5$. In that case the curve (d) would be flat as well with $\Pi_{U>}^{B<}(n) = \epsilon_\eta$ for $k > 2$. Instead, there is a drop of $\Pi_{U>}^{U<}(n)$ compensated by a symmetric bump of $\Pi_{U>}^{B<}(n)$ for $2 < \log_{10} k < 4.5$. This drop of $\Pi_{U>}^{U<}(n)$ is consistent with a spectrum steeper than $k^{-2/3}$. Indeed, the bump of $\Pi_{U>}^{B<}(n)$ corresponds to some extra energy taken from ϵ and dissipated by Joule effect. Then there is less energy to be transferred through the kinetic energy cascade. The physical reason why this scenario happens for scales just larger than the resistive scale, however is still unclear.

For the parameters of Fig. 5 the Kolmogorov dissipation scales are given by $k_\eta = (\epsilon/\eta^3)^{1/4} = 10^{4.5}$ and $k_\nu = (\epsilon/\nu^3)^{1/4} = 10^{6.75}$ which correspond quantitatively well with the beginning of the second and third plateau of $\Pi_{tot}(n)$. This shows that the arguments leading to the Kolmogorov dissipation scales (see next section) are not affected by the change of spectra slopes observed in Fig. 4.

Finally for completeness, we produced three movies showing the time evolution of the spectra of the other quadratic quantities. In u-helicity.mpg, b-helicity.mpg and cross-helicity.mpg, $\log_{10} \mathcal{H}_U(n)$, $\log_{10} \mathcal{H}_B(n)$ and $\log_{10} \mathcal{H}_C(n)$ are plotted versus $\log_{10} k$ where the blue and red dots denote positive and negative signs.

4.3 Dissipation scales ratio

At the end of section 2.3 we have already explained how we identify the viscous and resistive scales k_ν and k_η , by comparing the turn over time to the respective dissipative times. In Fig. 6 we plot the ratio k_ν/k_η versus $\text{Pm} \leq 1$ for different values of Re . We find that $k_\nu/k_\eta \sim \text{Pm}^{-3/4}$. To understand why, it is sufficient to say that between k_η and k_ν the kinetic energy obeys a Kolmogorov

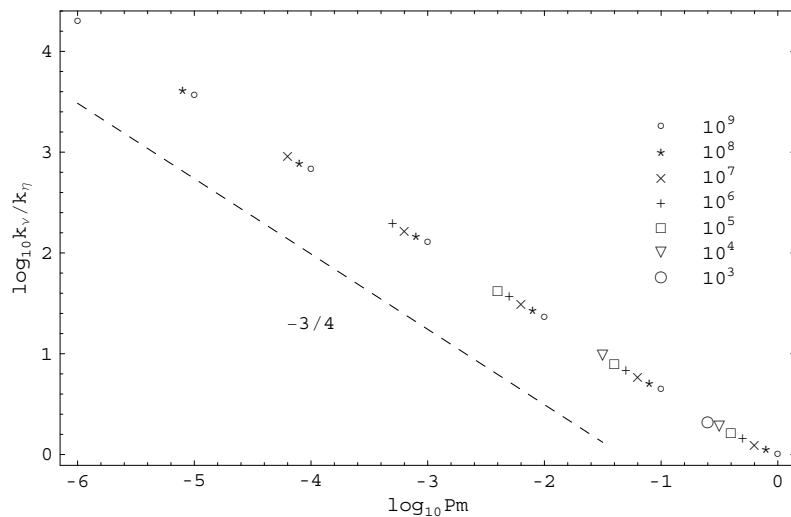


Figure 6. Ratio k_ν/k_η versus Pm for different values of ν^{-1} indicated in the legend. The straight line $k^{-3/4}$ is plotted (dashed line) for comparison.

spectrum $U(k) = \epsilon^{1/3}k^{-1/3}$ (see Fig. 4), leading to $\tau_U^{-1} = kU(k) = \epsilon^{1/3}k^{2/3}$. Comparing τ_U^{-1} with respectively $\tau_\nu^{-1} = \nu k^2$ and $\tau_\eta^{-1} = \eta k^2$ leads [47] to the dissipation scales $k_\nu \sim (\nu^3/\epsilon)^{-1/4}$ and $k_\eta \sim (\eta^3/\epsilon)^{-1/4}$. This in turn leads to a dissipation scales ratio in $\text{Pm}^{-3/4}$.

4.4 Route to saturation

In this section we study the influence of Pm on the way the dynamo saturates. For that we calculate the ratio of magnetic to kinetic energy E_B/E_U , E_B and E_U being defined as in (12). In Fig. 7, E_B/E_U is plotted versus Rm for three values of Pm. We note that for Rm much larger than the critical value, the level of saturation E_B/E_U may go beyond 1 for $\text{Rm} \sim 10^5$. Such a super saturation state could be expected from the spectra of Fig. 4. At the threshold, the slope of E_B/E_U versus Rm follows a turbulent scaling of the form $E_B/E_U \sim (\text{Rm} - \text{Rm}_c)/\text{Rm}_c^2$ as expected by Pétrélis and Fauve [49]. Indeed as in this case the threshold Rm_c does not vary very much with Pm, the slopes at $\text{Rm} = \text{Rm}_c$ are similar. This is to contrast with the laminar scaling $E_B/E_U \sim \text{Pm}(\text{Rm} - \text{Rm}_c)/\text{Rm}_c^2$ [49] which would lead to a quasi-horizontal slope for $\text{Pm} = 10^{-4}$.

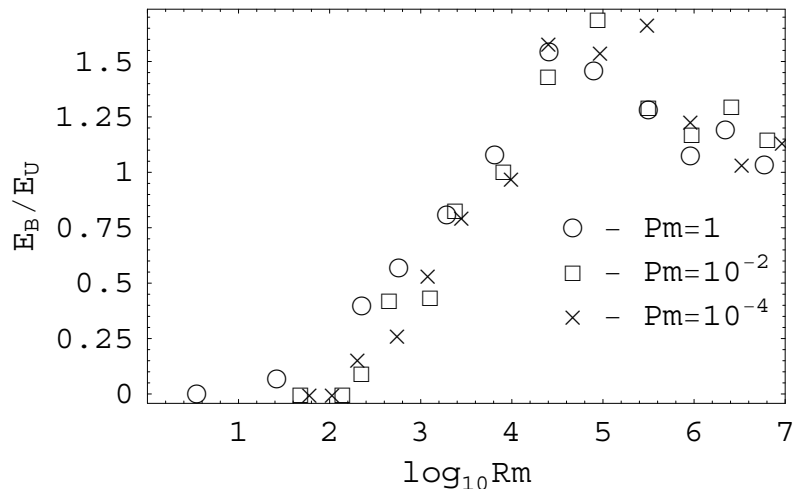


Figure 7. The energy ratio E_B/E_U versus Rm for $n_f = 4$ and three values of Pm .

4.5 Dynamo threshold

In Fig. 8 the dynamo threshold Rm_c is plotted versus Pm^{-1} for $n_f = 4$. For increasing values of Pm^{-1} up to 10^3 the threshold first increases in accordance with previous direct numerical simulations [4, 5, 6, 7, 8, 9]. However, for values of Pm^{-1} larger than 10^3 the threshold Rm_c is found to reach a plateau.

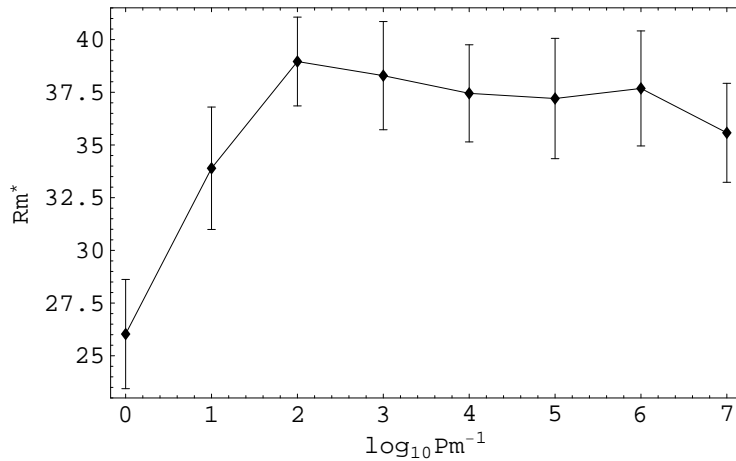
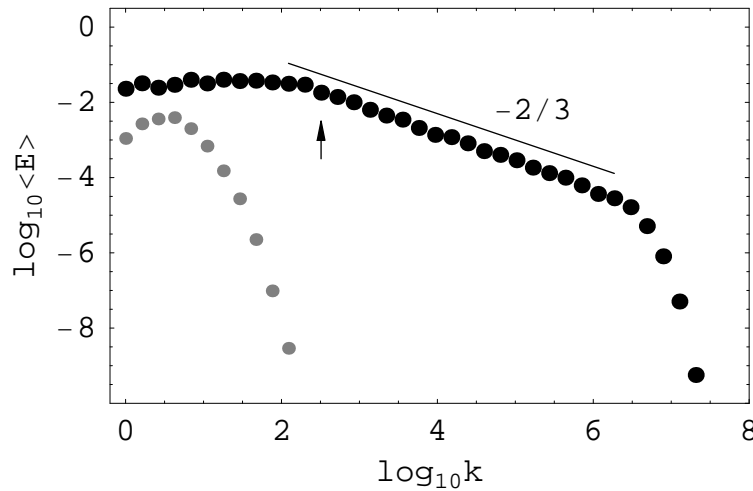
For each value of Pm , the vertical bar around Rm_c corresponds to values of Rm for which the magnetic solution is erratic. In other words, below the bars there is no dynamo action and above the bars there is a well define statistically stationary magnetic solution. In between though we do not observe intermittency as in [50, 51], the dynamo is irregular, the mean magnetic energy increasing and decreasing versus time.

4.6 Influence of a forcing scale smaller than the resistive dissipation scale

In Fig. 9, the kinetic and magnetic spectra are plotted for a forcing scale smaller than the resistive scale k_η . In that case the inertial range does not play a role in the magnetic generation and a kinetic spectra in $k^{-2/3}$ is recovered.

5 Discussion

In this paper we investigated the fully developed MHD turbulence at magnetic Prandtl number lower than unity, using a shell model of MHD turbulence with an appropriate forcing. The main results are:


 Figure 8. Dynamo threshold Rm_c versus Pm^{-1} for $n_f = 4$.

 Figure 9. Kinetic (black dots) and magnetic (gray dots) stationary spectra for $\nu = 10^{-9}$, $Pm = 10^{-7}$ and a forcing scale corresponding to $n_f = 12$. See also the movie `energy2.mpg` in which $\log_{10} E^U(n)$ and $\log_{10} E^B(n)$ are plotted versus $\log_{10} k$ with respectively red and blue dots.

1. For strong MHD turbulent dynamo states (large Rm) we find kinetic and magnetic energy spectra close to the Kolmogorov spectrum $k^{-2/3}$ except at scales just larger than the resistive dissipation scale for which there is a weaker (stronger) slope of the kinetic (magnetic) spectrum. This corresponds to the work of the Lorentz forces which increases with k up to $k = k_\eta$.
2. The evaluation of the viscous and resistive dissipation scales are consistent with Kolmogorov estimates leading to $k_\nu/k_\eta \sim Pm^{-3/4}$.
3. At the dynamo threshold Rm_c , the ratio of magnetic to kinetic energy scales

like $E_B/E_U \sim (\text{Rm} - \text{Rm}_c)/\text{Rm}_c^2$, as predicted by a turbulent scaling [49].

4. At very low values of Pm , the dynamo threshold Rm_c reaches a plateau.

Of course all these results rely on the assumption that the interactions between the different scales of motion and magnetic field are local interactions, each shell interacting with a few shells above and below. We believe that this should not make much difference as long as Pm is small, the Kolmogorov turbulence being governed by local interaction. In the other hand our results can not being tested against the Iroshnikov-Kraichnan $k^{-3/2}$ Fourier spectrum prediction [52] resulting from non local interactions between the flow and some large scale magnetic field which could result for example from dynamo action. By the way we believe that the $k^{-3/2}$ slope in FS98 is due to a lack of statistics as can be seen from the energy fluxes which are not flat and from the corresponding small range of scales. Adding some non local interaction with a large scale magnetic field in a local shell model, Biskamp [34] found a $k^{-3/2}$ slope, though taking only one such a non local interaction is somewhat artificial. Recently Verma [53] revisited the Iroshnikov-Kraichnan theory in which he shows that the large scale magnetic field becomes renormalized due to the nonlinear term, leading back to the Kolmogorov spectrum. This emphasizes the need for a complete nonlocal shell model in which any shell could interact with the others. This could be a good test against one theory or the other. Such a model would be also welcome for simulations at large Pm . Indeed at large Pm we expect the more energetic scales of the flow, corresponding to scales close to the viscous scales, to interact directly with the smaller scales of the magnetic field. Our local shell model can not catch such features and this is why we did not show results at large Pm for they surely lack physical ground. A further issue that could be addressed by a nonlocal shell model could be to distinguish between a large scale field generated by a small scale velocity field resulting from non local interactions (developed in the mean field formalism) and a large scale field generated by an "inverse cascade" as for example in Fig. 3 or in [54], resulting from local interactions. Concerning our local model, we believe that the results presented in Fig. 8 showing that the dynamo threshold does not depend on Pm at low values of Pm would stay qualitatively the same if additional nonlocal interactions were included in the model. Indeed the dynamo threshold corresponds to the growth start of the magnetic field which is then still not significant. Therefore any non local interactions (e.g. Alfvén sweeping effect) might not change the threshold.

6 Acknowledgments

Most of this work was done during a stay of R. S. at the LEGI, with a grant from the Université Joseph Fourier, Grenoble, France and completed during the visit of F.P. at the ICMM, Perm, Russia, supported by the ECO-NET program 10257QL. R.S. is also thankful for support from the BRHE program.

7 Appendix

For the pure hydrodynamic case ($B_n = 0$), only the two first conditions (8) and (9) are necessary to derive the forcing equations. In that case the forcing set writes

$$f_0 = \frac{\lambda \varepsilon}{(\lambda + 1)u_0 \cos(\phi_0 - \omega_0)} \quad (30)$$

$$f_1 = \frac{\varepsilon}{(\lambda + 1)u_1 \cos(\phi_1 - \omega_1)} \quad (31)$$

$$f_2 = 0, \quad (32)$$

while for the full MHD case the forcing set is derived from the three conditions (8), (9) and (10)

$$\begin{aligned} \frac{A}{\varepsilon}(1 + \lambda)f_0 &= \lambda b_2 u_1 \cos(\theta_2 - \phi_2) \cos(\phi_1 - \omega_1) \\ &\quad + \lambda^2 b_1 u_2 \cos(\theta_1 - \phi_1) \cos(\phi_2 - \omega_2) \end{aligned} \quad (33)$$

$$\begin{aligned} \frac{A}{\varepsilon}(1 + \lambda)f_1 &= b_2 u_0 \cos(\theta_2 - \phi_2) \cos(\phi_0 - \omega_0) \\ &\quad - \lambda^2 b_0 u_2 \cos(\theta_0 - \phi_0) \cos(\phi_2 - \omega_2) \end{aligned} \quad (34)$$

$$\begin{aligned} \frac{A}{\varepsilon}(1 + \lambda)f_2 &= -b_1 u_0 \cos(\theta_1 - \phi_1) \cos(\phi_0 - \omega_0) \\ &\quad - \lambda b_0 u_1 \cos(\theta_0 - \phi_0) \cos(\phi_1 - \omega_1) \end{aligned} \quad (35)$$

where

$$\begin{aligned} A &= b_2 u_0 u_1 \cos(\theta_2 - \phi_2) \cos(\phi_0 - \omega_0) \cos(\phi_1 - \omega_1) \\ &\quad + (\lambda - 1) b_1 u_0 u_2 \cos(\theta_1 - \phi_1) \cos(\phi_0 - \omega_0) \cos(\phi_2 - \omega_2) \\ &\quad - \lambda b_0 u_1 u_2 \cos(\theta_0 - \phi_0) \cos(\phi_1 - \omega_1) \cos(\phi_2 - \omega_2) \end{aligned} \quad (36)$$

and where u_j and ω_j (resp. b_j and θ_j) are the complex modulus and argument of U_{n_f+j} (resp. B_{n_f+j}).

References

- [1] G. Rüdiger and R. Hollerbach, 2004, The magnetic Universe, *Wiley-VCH*.
- [2] A.A. Schekochihin, S.C. Cowley and S.F. Taylor 2004, Simulations of the small-scale turbulent dynamo, *ApJ* **612** 276.
- [3] Y. Ponty, P.D. Mininni, A. Pouquet, H. Politano, D.C. Montgomery and J.-F. Pinton, 2005, Numerical study of dynamo action at low magnetic Prandtl numbers, *Phys. Rev. Lett.* **94** 164502.
- [4] A. Nordlund, A. Brandenburg, R.L. Jennings, M. Rieutord, J. Ruokolainen, R. Stein and I. Tuominen, 1992, Dynamo action in stratified convection with overshoot, *Astrophys. J.*, **392** 647.
- [5] A. Brandenburg, R.L. Jennings, A. Nordlund, M. Rieutord, R. Stein and I. Tuominen, Magnetic structures in a dynamo simulation, 1996, *J. Fluid Mech.*, **306** 325.
- [6] C. Nore, M.E. Brachet, H. Politano and A. Pouquet, 1997, Dynamo action in the Taylor–Green vortex near threshold, *Phys. Plasmas*, **4** 1.
- [7] U. Christensen, P. Olson and G.A. Glatzmaier, 1999, Numerical modeling of the geodynamo: a systematic parameter study, *Geophys. J. Int.*, **138** 393.
- [8] T.A. Yousef, A. Brandenburg and G. Rüdiger, 2003, Turbulent magnetic Prandtl number and magnetic diffusivity quenching from simulations, *Astron. Astrophys.*, **411** 321.
- [9] A.A. Schekochihin, S.C. Cowley, J.L. Maron and J.C. McWilliams, 2004, Critical magnetic Prandtl number for small-scale dynamo *Phys. Rev. Lett.*, **92** 54502.
- [10] I. Rogachevskii and N. Kleeorin, 2004, Nonlinear theory of a “shear-current” effect and mean-field magnetic dynamos *Phys. Rev. E*, **70** 046310.
- [11] A. Gailitis, O. Lielausis, S. Dementiev, E. Platacis, A. Cifersons, G. Gerbeth, Th. Gundrum, F. Stefani, M. Christen, H. Hänel and G. Will, 2000, Detection of a Flow Induced Magnetic Field Eigenmode in the Riga Dynamo Facility, *Phys. Rev. Lett.*, **84** 4365.
- [12] A. Gailitis, O. Lielausis, E. Platacis, S. Dementiev, A. Cifersons, G. Gerbeth, Th. Gundrum, F. Stefani, M. Christen and G. Will, 2001, Magnetic Field Saturation in the Riga Dynamo Experiment, *Phys. Rev. Lett.*, **86** 3024.
- [13] R. Stieglitz and U. Müller, 2001, Experimental demonstration of a homogeneous two-scale dynamo, *Phys. Fluids*, **13** 561.
- [14] U. Müller, R. Stieglitz and S. Horanyi, 2004, A two-scale hydromagnetic dynamo experiment, *J. Fluid Mech.*, **498** 31-71.
- [15] M. Bourgoin, L. Marié, F. Pétrélis, C. Gasquet, A. Guigon, J.-B. Luciani, M. Moulin, F. Namer, J. Burgete, A. Chiffaudel, F. Daviaud, S. Fauve, P. Odier and J.-F. Pinton, 2002, Magnetohydrodynamics measurements in the von Karman sodium experiment, *Phys. Fluids*, **14** 3046-3058.
- [16] F. Ravelet, A. Chiffaudel, F. Daviaud and J. Léorat, 2005, Towards an experimental von Karman dynamo: numerical studies for an optimized design, *Phys. Fluids*, submitted.
- [17] P. Frick, V. Noskov, S. Denisov, S. Khripchenko, D. Sokoloff, R. Stepanov, A. Sukhanovsky, 2002, Non-stationary screw flow in a toroidal channel: way to a laboratory dynamo experiment, *Magnetohydrodynamics*, **38**, 143-162
- [18] C. Normand, 2003, Ponomarenko dynamo with time-periodic flow, *Phys. Fluids*, **15** 1606-1611.
- [19] N. Leprovost, 2004, Influence des petites chelles sur la dynamique grande chelle en turbulence hydro et magnétohydrodynamique, *PhD thesis*, **Paris 6**.
- [20] R. Stepanov and K.-H. Rädler, 2004, The dynamo in a turbulent screw flow, *Advances in Turbulence X (Proceedings of the Tenth European Turbulence Conference)*, 789-792
- [21] J.-P. Laval, P. Blaineau N. Leprovost, B. Dubrulle and F. Daviaud 2006, Influence of turbulence on the dynamo threshold, *submitted*.
- [22] G.O. Roberts, 1972, Spatially periodic dynamos, *Phil. Trans. R. Soc. Lond. A*, **271** 411.
- [23] Y. B. Ponomarenko, 1973, Theory of the hydromagnetic generator, *J. Appl. Mech. Tech. Phys.*, **14** 775-778.
- [24] M.L. Dudley and R.W. James, 1989, Time-dependent kinematic dynamos with stationary flows, *Proc. R. Soc. Lond. A*, **425** 407-429.
- [25] R.M. Kulsrud and S.W. Anderson, 1992, Time-dependent kinematic dynamos with stationary flows, *Astrophys. J.*, **396** 606.
- [26] S. Boldyrev and F. Cattaneo, 2004, Magnetic-field generation in Kolmogorov turbulence, *Phys. Rev. Lett.*, **92** 144501.

- [27] J. Léorat, A. Pouquet and U. Frisch, 1981, Fully developed MHD turbulence near critical magnetic Reynolds number, *J. Fluid Mech.*, **104** 419-443.
- [28] P. Frick and D. Sokoloff, 1998, Cascade and dynamo action in a shell model of magnetohydrodynamic turbulence, *Phys. Rev. E*, **57** 4155.
- [29] P. G. Frick, 1983, Two-dimensional MHD turbulence. Hierarchical Model, *Magn. Hidrodin.*, **1** 60 [Magnetohydrodynamics **20**, 262 (1984)].
- [30] C. Gloaguen, J. Léorat, A. Pouquet and R. Grappin, 1985, A scalar model for MHD turbulence, *Physica D*, **51** 154.
- [31] R. Grappin, J. Léorat and A. Pouquet, 1986, *J. Phys. (France)*, **47** 1127.
- [32] V. Carbone and P. Veltri, 1990, *Geophys. Astrophys. Fluid Dynam.*, **52** 153.
- [33] V. Carbone, 1994, Scale similarity of the velocity structure functions in fully developed magnetohydrodynamic turbulence, *Phys. Rev. E*, **50** 671 [Eurphys. Lett. **27**, 581 (1994)].
- [34] D. Biskamp, 1994, Cascade models for magnetohydrodynamic turbulence, *Phys. Rev. E*, **50** 2702.
- [35] A. Brandenburg and K. Enquist and P. Olesen, 1996, Large-scale magnetic field from hydromagnetic turbulence in the very early universe, *Phys. Rev. D*, **54** 1291.
- [36] E.B. Gledzer, 1973, System of hydrodynamic type admitting two quadratic integrals of motion, *Dokl. Akad. Nauk. SSSR*, **209** 1046 [Sov. Phys. Dokl. **18**, 216 (1973)].
- [37] M. Yamada and K. Ohkitani, 1987, Lyapunov spectrum of a chaotic model of three-dimensional turbulence, *J. Phys. Soc. Jpn.*, **56** 4210.
- [38] U. Frisch, 1995, Turbulence, the legacy of A.N. Kolmogorov, (Cambridge University Press, Cambridge).
- [39] L. Biferale, 2003, Shell model of energy cascade in turbulence, *Annu. Rev. Fluid Mech.*, **35** 441-468.
- [40] Ya. B. Zeldovich, 1956, The magnetic field in the two-dimensional motion of a conducting turbulent fluid, *Zh. Eksp. Teor. Fiz.*, **31** 154 [Sov. Phys. JETP **4**, 460 (1957)].
- [41] P. Giulani and V. Carbone, 1998, A note on shell models for MHD turbulence, *Europhys. Lett.*, **43** 527-532.
- [42] S.A. Lozhkin, D.D. Sokolov and P.G. Frik, 1999, Magnetic Prandtl number and the small-scale MHD dynamo, *Astron. Rep.*, **43** 753-758.
- [43] G.K. Batchelor, 1950, On the spontaneous magnetic field in a conducting liquid in turbulent motion, *Proc. R. Soc. London A*, **201** 405.
- [44] V. L'vov, E. Podivilov, A. Pomyalov, I. Procaccia and D. Vandembroucq, 1998, Improved shell model of turbulence, *Phys. Rev. E*, **58** 1811.
- [45] L. Kadanoff, D. Lohse, J. Wang and R. Benzi, 1995, Scaling and dissipation in the GOY shell model, *Phys. Fluids*, **7** 617-29.
- [46] M. K. Verma, 2004, Statistical theory of magnetohydrodynamic turbulence: recent results, *Phys. Reports*, **401** 229-380.
- [47] R.H. Kraichnan and S. Nagarajan, 1967, Growth of turbulent magnetic field *Phys. Fluids*, **10** 859.
- [48] W. Dobler, N. Haugen, T. Yousef and A. Brandenburg 2004, Bottleneck effect in three-dimensional turbulence simulations, *Phys. Rev. E*, **68** 026304.
- [49] F. Pétrélis and S. Fauve, 2001, Saturation of the magnetic field above the dynamo threshold, *Eur. Phys. J. B*, **22** 273-276.
- [50] N. Leprovost and B. Dubrulle, 2005, The turbulent dynamo as an instability in a noisy medium, *Eur. Phys. J. B*, **44** 395-400.
- [51] N. Leprovost, B. Dubrulle and F. Plunian 2006, Instability in presence of noise: the example of homopolar dynamo, *submitted to Magnetohydrodynamics*.
- [52] D. Biskamp 2003, Magnetohydrodynamic Turbulence, (Cambridge University Press, Cambridge).
- [53] M. K. Verma, 1999, Mean magnetic field renormalization and Kolmogorov's energy spectrum in magnetohydrodynamic turbulence, *Phys. Plasmas*, **6** 1455-1460.
- [54] A. Pouquet, U. Frisch and J. Léorat, 1976, Strong MHD helical turbulence and the non linear dynamo effect, *J. Fluid Mech.*, **77** 321-354.